
Time resolved spectroscopic observations of an M-dwarf flare star EV Lacertae during a flare

Satoshi Honda¹, Yuta Notsu², Kosuke Namekata², Shota Notsu², Hiroyuki Maehara³, Kai Ikuta², Daisaku Nogami², and Kazunari Shibata^{2,4}

¹Nishi-Harima Astronomical Observatory, Center for Astronomy, University of Hyogo, 407-2, Nishigaichi, Sayo-cho, Sayo, Hyogo 679-5313, Japan

²Department of Astronomy, Kyoto University, Kitashirakawa-Oiwake-cho, Sakyo-ku, Kyoto 606-8502

³Okayama Observatory, Kyoto University, 3037-5 Honjo, Kamogata, Asakuchi, Okayama 719-0232, Japan

⁴Astronomical Observatory, Kyoto University, Kitashirakawa-Oiwake-cho, Sakyo-ku, Kyoto 606-8502, Japan

*E-mail: honda@nhao.jp

Received (reception date); Accepted (acceptation date)

Abstract

We have performed 5 night spectroscopic observation of the $H\alpha$ line of EV Lac with a medium wavelength resolution ($R \sim 10,000$) using the 2m Nayuta telescope at the Nishi-Harima Astronomical Observatory. EV Lac always possesses the $H\alpha$ emission line; however, its intensity was stronger on August 15, 2015 than during other four-night periods. On this night, we observed a rapid rise (~ 20 min) and a subsequent slow decrease (~ 1.5 h) of the emission-line intensity of $H\alpha$, which was probably caused by a flare. We also found an asymmetrical change in the $H\alpha$ line on the same night. The enhancement has been observed in the blue wing of the $H\alpha$ line during each phase of this flare (from the flare start to the flare end), and absorption components were present in its red wing during the early and later phases of the flare. Such blue enhancement (blue asymmetry) of the $H\alpha$ line is sometimes seen during solar flares, but only during the early phases. Even for solar flares, little is known about the origin of the blue asymmetry. Compared with solar-flare models, the presented results can lead to the

understanding of the dynamics of stellar flares.

Key words: stars: flare — stars: individual: EV Lacertae —stars: chromospheres — stars: activity —
line: profile

1 Introduction

Solar flares are energetic explosions in the solar atmosphere around active regions. They are considered to be caused by the energy release through magnetic reconnections in the corona (e.g., Shibata & Magara 2011). The flare energy, which is released in the corona and transported into the lower atmospheres, is dissipating in the dense chromosphere. This produces intense heating, which in turn leads to the evaporation and condensation processes. Flares are observed across the entire electromagnetic spectrum from radio emission to high-energy gamma-rays. Numerous observations of solar flares have been carried out in the coronal (e.g., X-ray) and chromospheric emission (e.g., $H\alpha$) bands so far (e.g., Shibata & Magara 2011). However, many of their aspects are yet to be investigated, both observationally and theoretically.

It is known that stellar flares occur on various types of stars. They are observed mainly as a rapid rise of the emission intensity (X-ray, optical, radio, etc.) followed by its slow decrease. In particular, young stars, close binary stars, and dMe stars can produce frequent flares (e.g., Hawley & Pettersen 1991, Kowalski et al. 2010), and sometimes produce “superflares”, i.e., flares whose total energy reaches values $10\text{-}10^6$ times larger than the largest flares observed from the Sun. Recent photometric data from the Kepler spacecraft found many superflare events on G, K, M-type stars (cf. Maehara et al. 2012, Shibayama et al. 2013, Notsu et al. 2013, Candelaresi et al. 2014, Hawley et al. 2014, Davenport 2016, Yang et al. 2017). These studies show many statistical properties of superflares. The energy-release process of such large stellar flares can be explained by magnetic reconnection (Shibata & Yokoyama 2002; Maehara et al. 2015; Namekata et al. 2017). However, several issues remain to be investigated, especially concerning the dynamics and radiation mechanisms present during such large flares.

Numerous spectroscopic studies of solar flares have been performed in order to understand the flare dynamics and their radiation mechanisms. The $H\alpha$ line is the most frequently observed line among solar flare spectroscopic observations. Red asymmetry (enhancement of the red wing) has been often observed in the $H\alpha$ line profile during solar flares (e.g., Ichimoto & Kurokawa 1984, Canfield et al. 1990, Kuridze et al. 2015). This is thought to be due to the the process known as

chromospheric condensation, which is the downflow of cool plasma in the flaring atmosphere. Blue asymmetry has also been observed in the early phase of flares (e.g., Canfield et al. 1990, Heinzel et al. 1994). This has been also observed in the Na I D1, Ca II 8542 (Kuridze et al. 2016; Kuridze et al. 2017) and Mg II h line (Tei et al. 2018). These results might mean the existence of cool plasma flows moving upward. However, the detailed explanation of this blue asymmetry is still controversial.

Such $H\alpha$ line asymmetries are also observed during stellar flares. Houdebine et al. (1993) found red asymmetries in the core and wings of Balmer lines during a flare from a late-type dMe star (AD Leo). They interpreted this as an evidence of downward chromospheric condensations, similar to those seen on the Sun. An example of asymmetries present in the blue wing was found during a flare from the dMe star AT Mic in Balmer and Ca II H and K line (Gunn et al. 1994b). In addition, blue asymmetry has been sometimes observed during stellar flares (e.g., YZ CMi; Gunn et al. 1994a, AD Leo; Crespo-Chacon et al. 2006, and DG CVn; Caballero-Garcia et al. 2015). With regards to YZ CMi, blue asymmetry has been observed also in the Mg II h line (Hawley et al. 2007).

However, previous spectroscopic observations of stellar flares are not sufficient to understand the mechanisms responsible for the red and blue asymmetries. We need detailed spectra with higher temporal resolution, which has not been shown in previous studies. This is because flares themselves are rare events and high-temporal resolution observations require continuous observation during a time-span longer than a few hours.

EV Lac (GJ 873) is a well-known M4.5eV single-flare star. From this star, superflares were also detected by X-ray (ASCA ; Favata et al. 2000) and Gamma-ray (Swift ; Osten et al. 2010) observations. Schmidt et al. (2012) showed the frequency of flares from EV Lac to be 0.094 (events/hour), based on photometric observations. These facts indicate that EV Lac is a promising target for the investigation of stellar flares.

In this paper, we present the results of spectroscopic observations of flares from EV Lac. The details of the spectroscopic observations are described in Sec.2. In Sec.3, we show the change of $H\alpha$ -equivalent widths and line profiles with high temporal resolution. These changes of the $H\alpha$ line are discussed in Sec.4.

2 Spectroscopic observations of EV Lac

The spectroscopic observations were carried out by the Nayuta 2m telescope at the Nishi-Harima Astronomical Observatory. The MALLS (Medium And Low-dispersion Long-slit Spectrograph) was used with a resolving power ($R = \lambda/\Delta\lambda$) of $\sim 10,000$ at 6500\AA . The wavelength range was $6350\text{--}6800\text{\AA}$. This region includes the $H\alpha$ (6562.8\AA) and He I (6678.2\AA) lines. The observation runs were

carried out on July 31, August 1, 15, 26, and 27, 2015. The integration times for the single spectra (per frame) were 3 or 5 minutes. The signal-to-noise ratio (S/N) of each observed spectrum was more than 50. The total duration of the observations were 1, 2.5, 5.5, and 3.5 hours on August 1, 15, 26, and 27, respectively. On July 31, only one frame of observation was conducted. The log of observations is shown in Table 1. Data reduction was done using the twodspec package of the IRAF¹ software in the standard manner (overscan correction, flat fielding, aperture determination, spectral extraction, sky subtraction, wavelength calibration, and normalization by the continuum). Figure 1 shows the spectrum of EV Lac obtained by MALLS on July 31 (quiescent phase, as described in Section 3.1). We can see the strong $H\alpha$ emission line, and many atomic lines, molecular bands (TiO, CaH, etc.). All observed spectra show similar features.

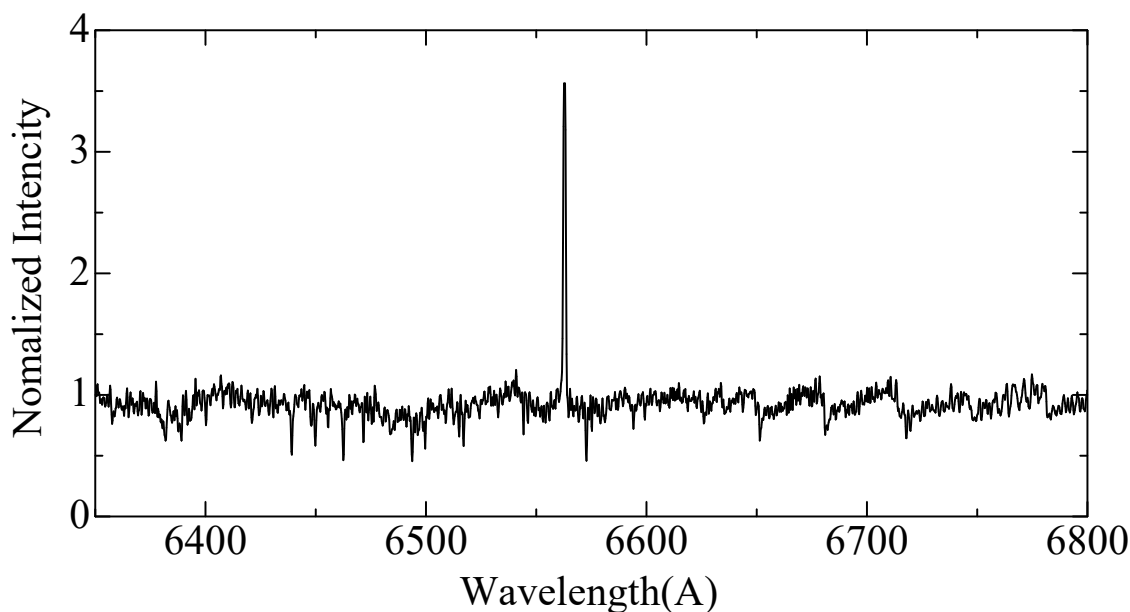


Fig. 1. Quiescent spectrum of EV Lac taken by MALLS on July 31, 2015. The strong emission line at the center of the spectrum is $H\alpha$. There are many atomic absorption lines and molecular bands present in this region.

3 Measurements of $H\alpha$ emission line

3.1 Equivalent width of $H\alpha$ emission line

We measured the equivalent width (E.W.) of the $H\alpha$ line in every spectrum in order to investigate the flare and stellar activity. For the measurement of the equivalent widths, the “e” command of the plot task in IRAF was used. We assumed the range of the $H\alpha$ emission line is from 6557.5 Å to 6567.5 Å, and integrated the flux above the continuum to measure the equivalent widths. The measured values

¹ IRAF is distributed by the National Optical Astronomy Observatories, which is operated by the Association of Universities for Research in Astronomy, Inc., under cooperate agreement with the National Science Foundation.

of the equivalent widths are shown in Table 2.

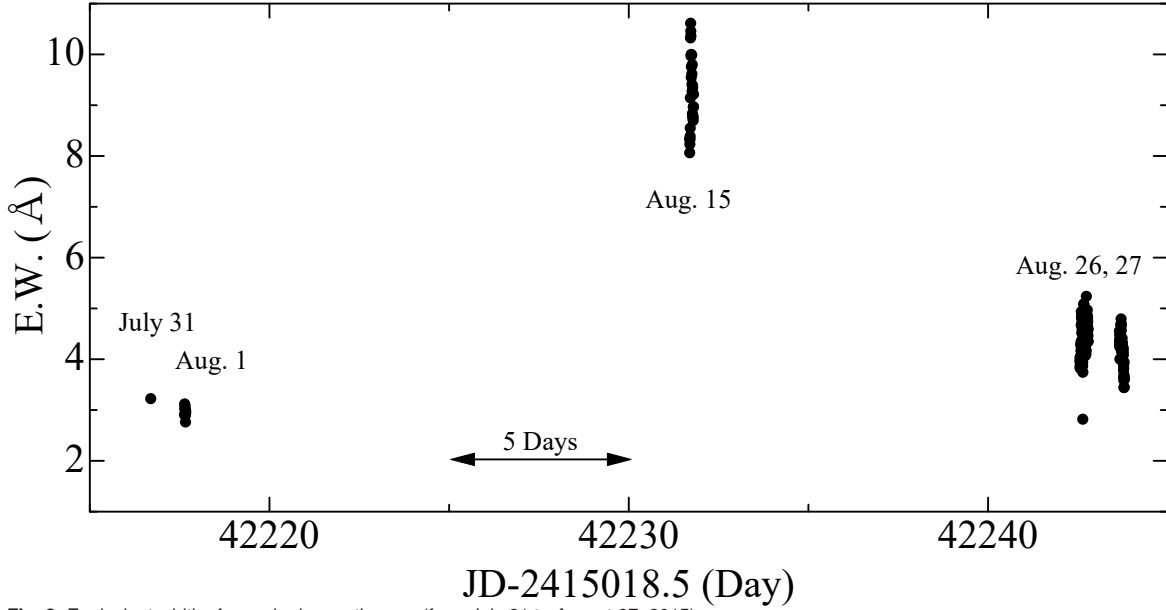


Fig. 2. Equivalent widths for each observation run (from July 31 to August 27, 2015).

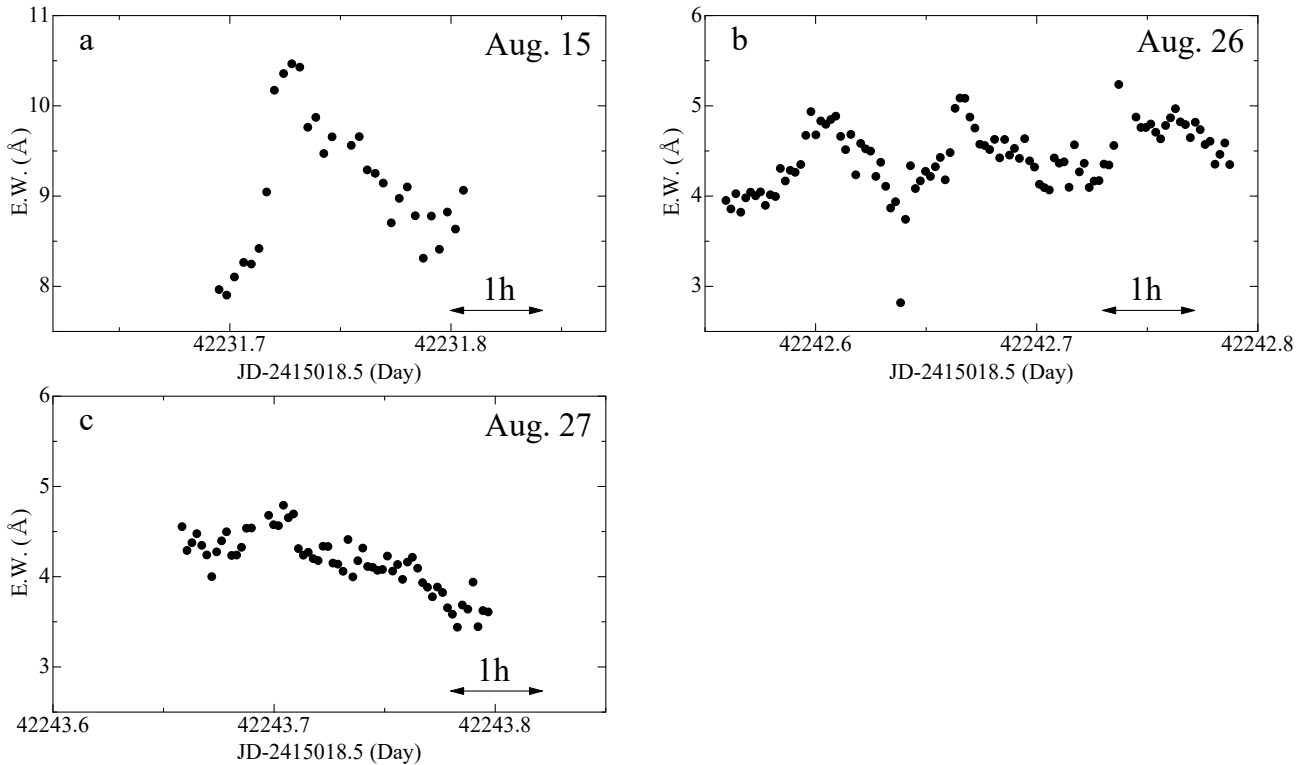


Fig. 3. Equivalent widths for each observation run (August 15, August 26, and August 27 respectively). August 26 observation (b) shows a short-term modulation. This period is much shorter than the stellar rotation period (4.4 days).

In Figures 2 and 3, we show the equivalent width of the $H\alpha$ line as a function of time for observation run. In the July 31 and August 1 spectra, the equivalent width did not show significant changes. The typical value of the equivalent width was about 3 \AA during these two periods. Baranovskii et al.

(2001) indicated that the $H\alpha$ equivalent widths of EV Lac are 3.5–5.3 Å in the quiescent state and 4.7–10.6 Å in the active state. On August 1, we have obtained the 10 frames continuously during a 1-hour period, with no observable changes of $H\alpha$ intensity. EV Lac was in a quiescent state during this period.

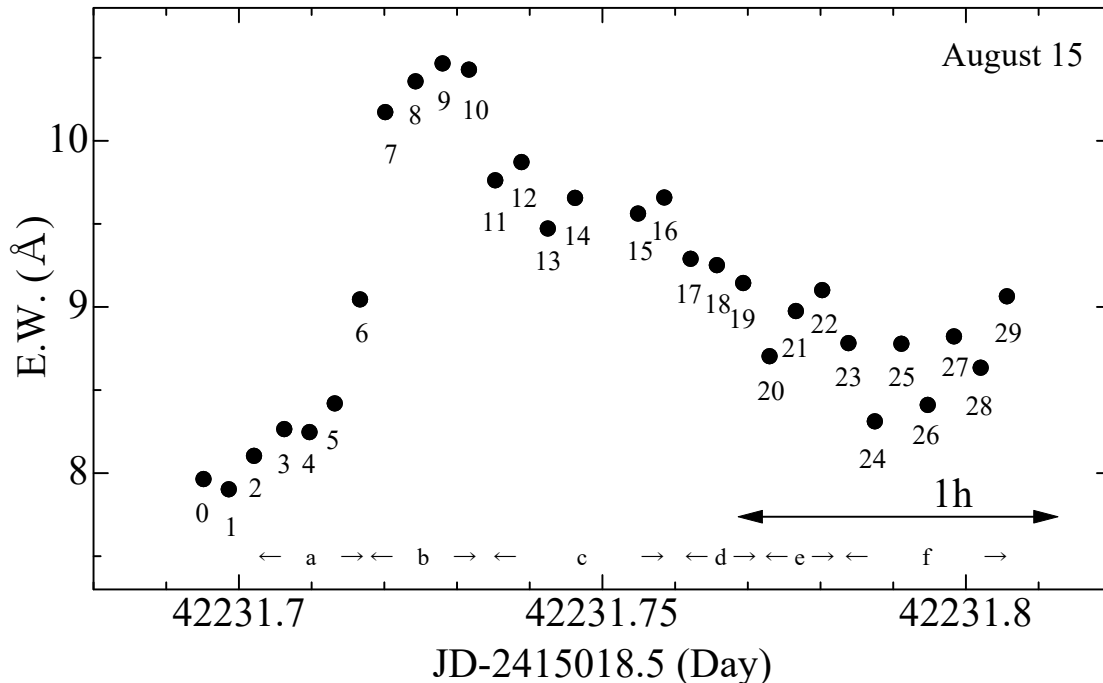


Fig. 4. Same as August 15 of figure 2, with each measurement labeled by numbers and the groups (see text for the details).

However, we found a substantial change of intensity of the $H\alpha$ line between July 31 and August 15. Figure 5 shows the comparison of two spectra, July 31 and August 15 (No.9 in Figure 4), in the region of the $H\alpha$ line. In the August 15 spectra, the equivalent width of the $H\alpha$ line showed large variations in the range of 8.1–10.5 Å. These results suggest that EV Lac was in an active state that night. In addition, the $H\alpha$ line showed a rapid rise followed by a slow decrease of intensity, which was probably caused by a long-duration flare. The enhanced $H\alpha$ emission is a common feature of solar and stellar flares (e.g., Haisch et al. 1991). It increased by 2 Å within 20 minutes and then slowly decreased during a period of 1.5 hours. This is a similar shape as possessed by typical light curves of solar flares. However, the present observation was a very long duration flare. The He I 6678 Å line is also present in each spectrum taken this night, although it was not observed on other nights. Figure 6 shows the spectra of the region around He I 6678 Å. This He emission can be a further evidence of the flare occurrence. The He I 5876 Å D3 line is well-known to show emission during flares. The He I 6678 Å line is expected to show the same behavior as the D3 line (e.g., Eason et al. 1992). However, it was too weak to discuss its changes of intensity during this night. We could not find any changes in other atomic and molecular lines.

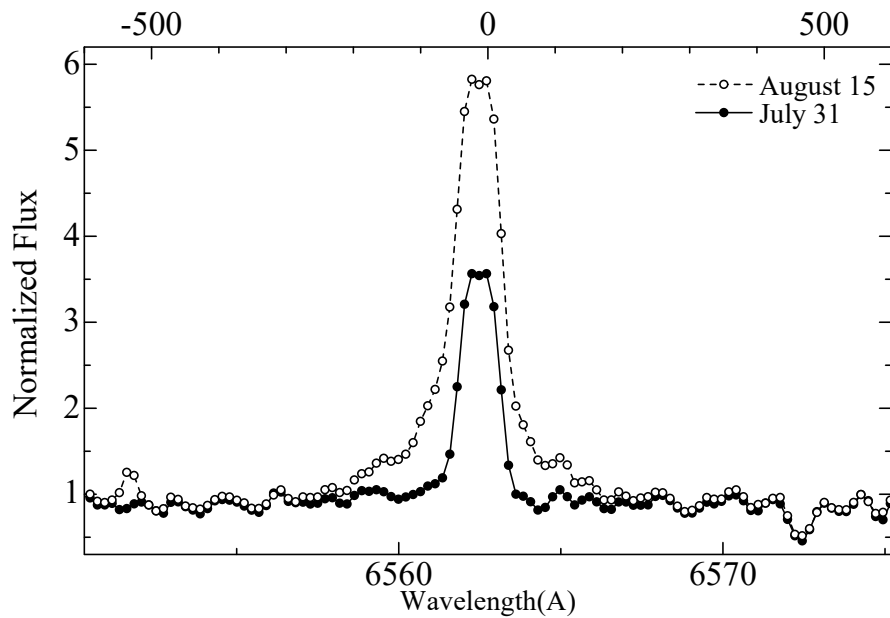


Fig. 5. Comparison of two spectra, from July 31 and August 15 (No.9 in Figure 4), respectively. The velocity is set to 0 km s^{-1} at the $\text{H}\alpha$ center (6562.81Å).

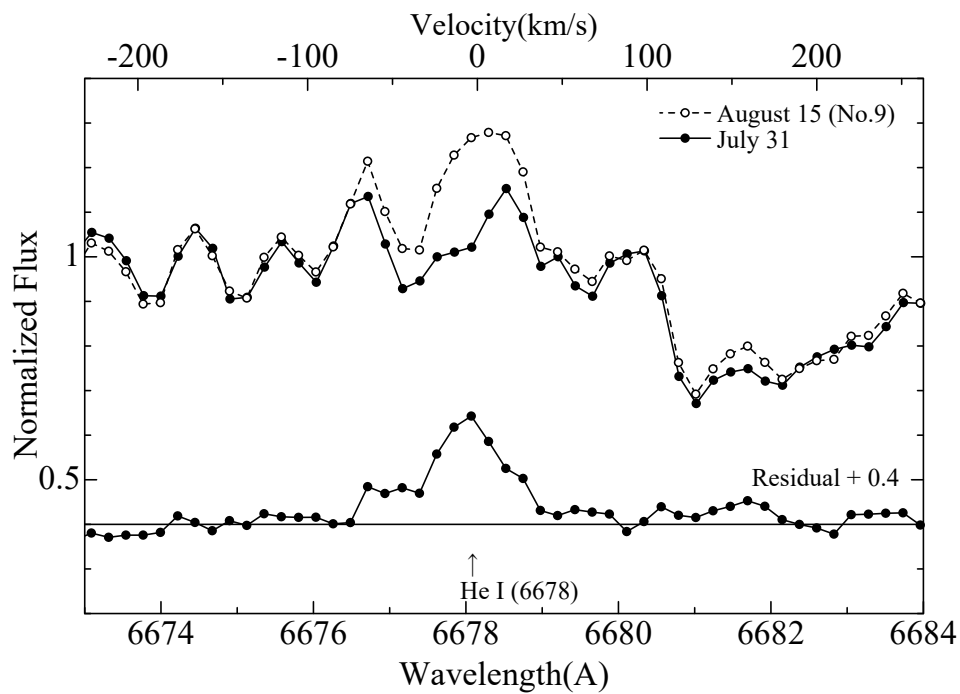


Fig. 6. Spectral comparison in the region around He I 6678.15 Å and the residual spectrum obtained by subtracting the July 31 spectra from August 15 (No.9). The value of the vertical axis of the residual spectrum is shifted by +0.4. The velocity is set to 0 km s^{-1} at the He I line center (6678.15Å).

The equivalent widths of H α line of August 26 and 27 were smaller than those of August 15. However, small changes were seen on those days as well (Figure 3). From the August 26 observation, it seems that three small flares occurred. However, no flares were seen during the August 27 observation. A typical value of the equivalent width of the H α line was 4.5 Å on those two days, which is in the range of the “quiescent state” (Baranovskii et al. 2001). Although the equivalent width of H α shows a gradual decrease on August 27, it might be due to the change of appearance of an active region with the rotation of a star. However, we also note that Pettersen (1980) suggest that the variations of the H α line do not correlate clearly with the rotation.

3.2 Profiles of H α line during August 15 flare

In the observations on August 15, we found a change in the H α line profile. Figure 7 shows the comparison of the weakest and strongest features of the H α line on this night. The time interval between No.1 and No.9 is 42 minutes. No clear shift of the line center wavelength was found. We found an enhancement of the wing component of the H α line in the blue region. The flux enhancement in the blue region around -100 km s^{-1} is clearly larger than that in the red region around $+100 \text{ km s}^{-1}$ (Figure 7, see also Figure 9b). The change in the line profile during the flare was stronger in the blue wing component of the line than in the red one. We discuss about this in detail in Section 4.

Previous studies (Johns-Krull et al. 1997) observed a solar flare with high-resolution spectroscopy and found that the H α emission line during the flare showed a double-peak profile. Martin (1999) showed that the H α line of the dMe star VB 8 has a double peaked profile, showing the variation of peak intensity ratio. Before the flare, the blue-peak intensity is stronger than that of the red peak. However, this peak intensity ratio is reversed during the flare. After the flare, the blue peak becomes stronger than the red, once again. Our observations of EV Lac also show the features of a double-peak profile for the H α line (Figure 7). The spectrum from July 31 shows the features of the same peak intensity ratio. However, the line had a variation of double-peak profile with the peak of red part having a more prominent emission than the blue in an August 15 spectrum (No.1). It seems that the peaks were reversed pre-flare and during the flare (Figure 7). This change of peak intensity ratio is the opposite of observations of VB 8 (Martin 1999), but it is not clear because of the insufficient wavelength resolution of the spectra. We must note that to compare the intensity ratio of double peaks, we need higher wavelength-resolution spectra. In the observations by Martin (1999), the wavelength-resolution of the spectra ($R = 110,000$) were higher than that in our observations ($R \sim 10,000$).

To clearly see the pure-flare components, we subtracted the pre-flare spectra. We assumed the

second spectrum (No.1 in Figure 4) of the series as a pre-flare spectrum, which showed the smallest equivalent width this night. Figure 8 shows the time series of the subtracted line profiles of $H\alpha$. The subtracted spectra show the variations in the emission and absorption components. Figure 9 shows that in the impulsive phase of the flare (Figure 9a: No. 2–6 in Figure 4), an increase of the intensity was observed in the blue wing of the line, and an absorption component was observed in the red wing. This absorption component with a velocity of a few tens of km s^{-1} exhibited a change of intensity in time. This absorption component does not correspond to the wavelength of the water vapor lines (6564.206 \AA). In the 4th spectrum (No.3), the red absorption component exhibits its strongest features. After that, the intensity of the blue component increased, together with the whole-emission component, while the red absorption decreased. In the 7th spectrum (No.6), the absorption component disappeared.

In the peak-phase spectra (Figure 9b), the profile did not change from the 8th (No.7) to 11th (No.10) spectra. In those spectra, the values of the equivalent width are more than 10 \AA , and no absorption features are observed.

The 12th (No.11) or later spectra showed a deficit of the red wing and the variations of intensity in the line center (Figure 9c : $10 \text{ \AA} > \text{E.W.} \gtrsim 9.5 \text{ \AA}$, Figure 9d : $9.5 \text{ \AA} > \text{E.W.}$).

The absorption component in the red wing appeared again in the 21th (No. 20) and later spectra (Figure 9e). Although those spectra are noisy (Figure 9f) because of bad weather, we can see that the enhancement of the blue part continued until the end of the observation.

4 Discussion

4.1 Variabilities of equivalent width of $H\alpha$ emission

The intensity of the $H\alpha$ line of EV Lac shows substantial changes. We can consider the following three possibilities to explain the change of the $H\alpha$ intensity: (1) the brightening by the flares (typical time scale of \sim hours); (2) visibility of the active region with the rotation of the star (rotation period = 4.4 days); (3) evolution of active regions (days \sim months). During our one-month observation period, EV Lac exhibited a change from its quiet phase to its active phase. Since the rotation period of EV Lac is 4.4 days (Pettersen 1980), roughly 50% of the stellar surface visible to the observer on August 1 would also be visible on August 15. This indicates that the change of the $H\alpha$ intensity might be caused by the visibility change of the active region via stellar rotation. We could not determine the origin of the change of the $H\alpha$ intensity from our observations. Several spectroscopic observations of EV Lac have been carried out with a focus on the $H\alpha$ line (e.g., Alekseev et al. 2003, Melikian et al. 2006), but there are very few observations with time cadence similar to that of our observation. If we

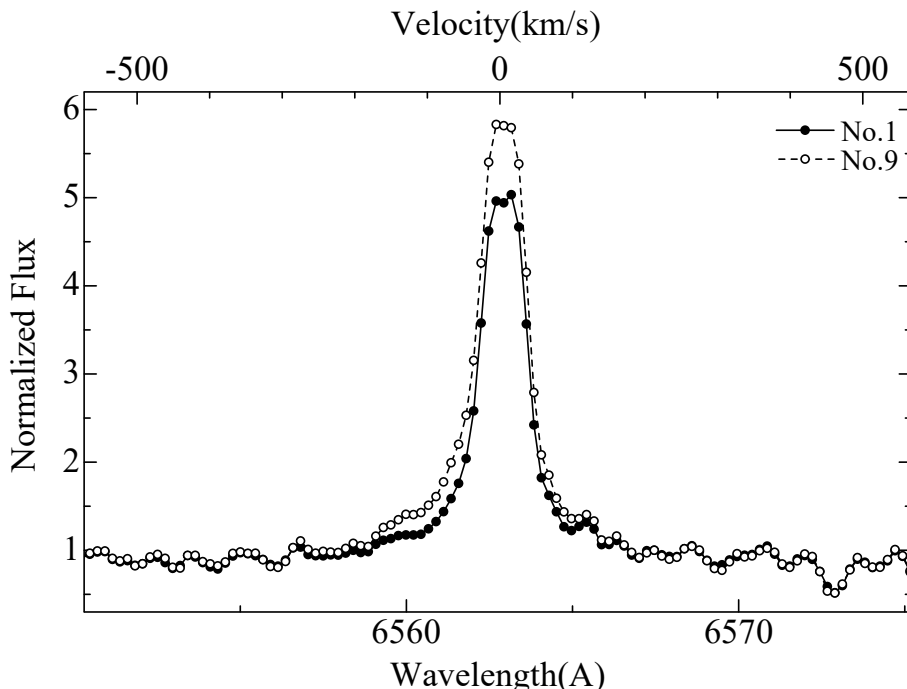


Fig. 7. Comparisons of spectra taken on August 15. The open circle and dashed line indicate the strongest line (No.9), the filled circle and solid line indicate the weakest line (No.1). The time interval between No.1 and No.9 is 42 minutes. The upper axis shows the velocity, lower axis the wavelength. The velocity is set to 0 km s^{-1} at $H\alpha$ line center (6562.81\AA).

aim to clarify the relationship between the fluctuations of line intensities and stellar activities, more frequent and long-term monitoring is necessary.

The large change in the equivalent width on August 15 may have been caused by a very long-duration flare. The equivalent width has already become larger than previously observed by the beginning of the flare. On this night, the active region of the stellar surface might have been large and flare might have occurred. Otherwise, a few huge flares or a lot of small flares occurred on the stellar surface before the large flare we observed. Simultaneous photometric data would be helpful to understand the variations of equivalent width of $H\alpha$. Unfortunately, we do not have the data of photometric observations for the observed periods. We note that we could not observe any filling-up of atomic lines even during the flare.

4.2 Line profile of $H\alpha$ emission during the flare

The change of the $H\alpha$ line profile is associated with the dynamics of the cool gas ($\sim 10,000 \text{ K}$) present in the flare. Blue asymmetry (enhancement of the blue $H\alpha$ emission wing), which was seen in our observations, is also observed at the early phase of solar flares. However, the mechanisms are still unknown. Several studies have been made on line profile asymmetries are produced in the solar flare models. Solar flare models obtained with the radiative hydrodynamic simulations show that

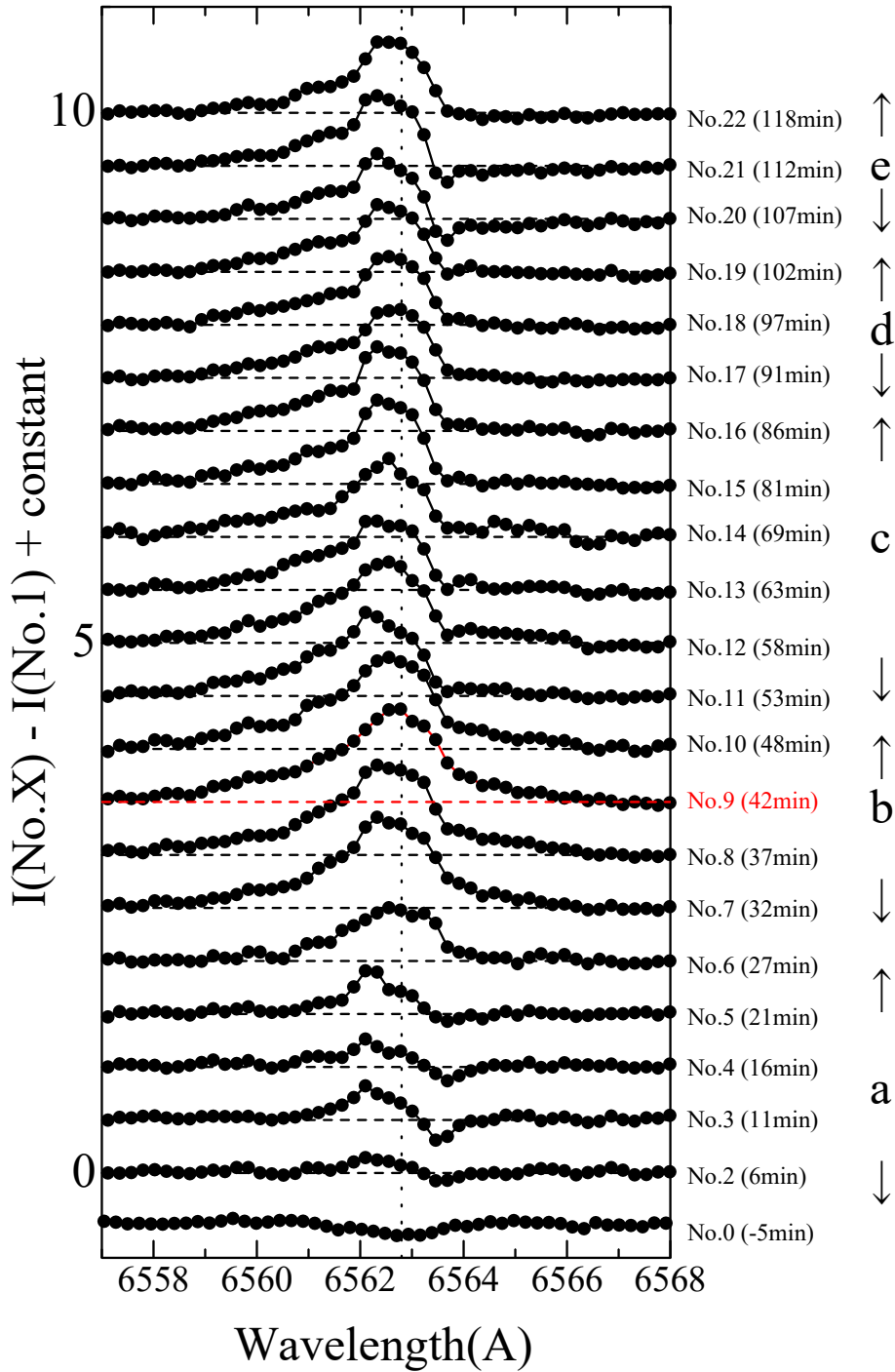


Fig. 8. Time sequence of subtracted line profiles of the spectra taken on August 15. (No.0–22).

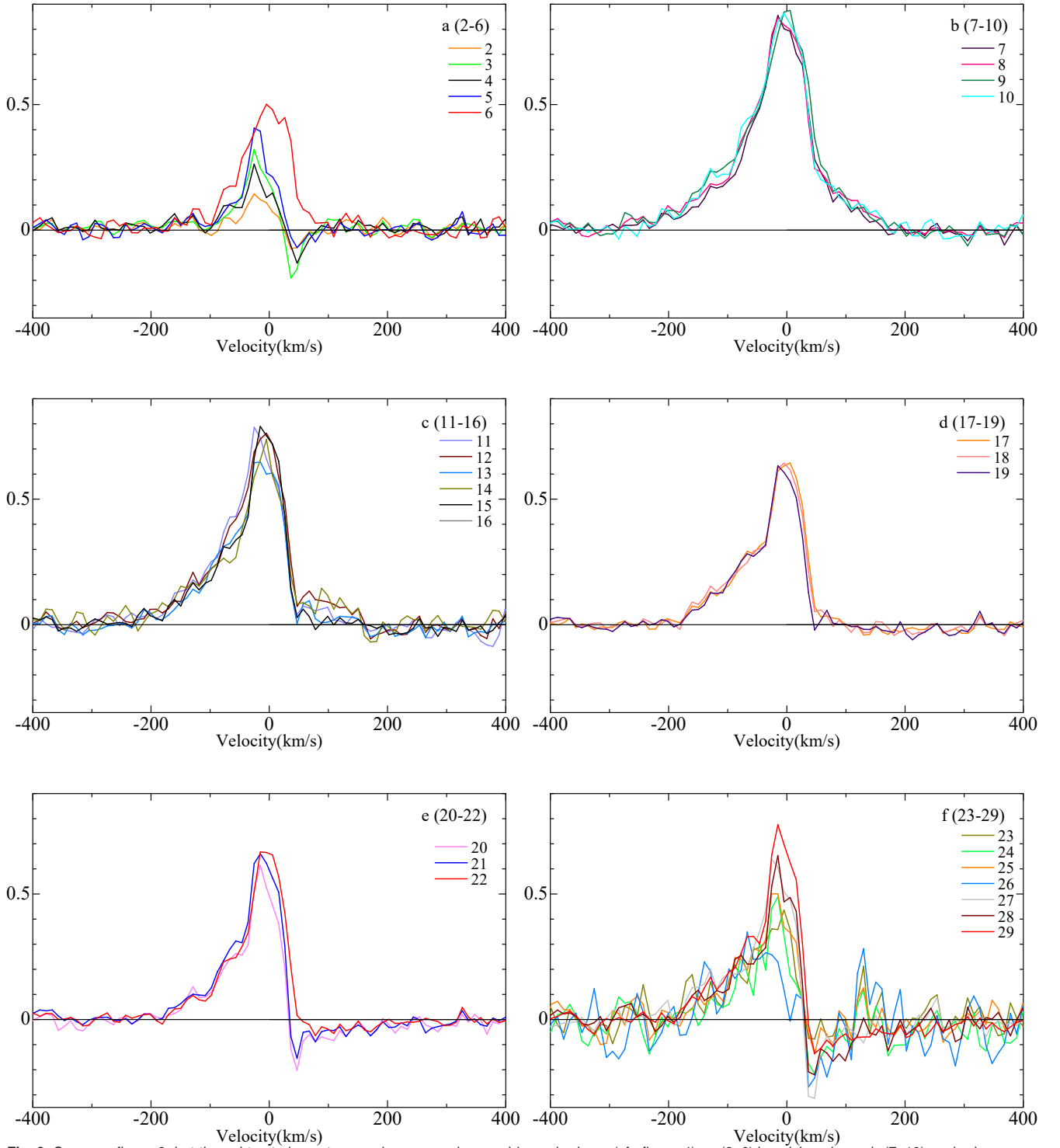


Fig. 9. Same as figure 8, but the subtracted spectra are shown superimposed in each phase (cf., figure 4). a (2–6):impulsive phase, b (7–10):peak phase ($E.W. > 10 \text{ \AA}$), c (11–16): decay phase ($10 \text{ \AA} > E.W. \gtrsim 9.5 \text{ \AA}$), d (17–19):decay phase ($9.5 \text{ \AA} > E.W.$), e (20–22):small absorption in red part, f (23–29):poor quality spectrum. (Color version of these figures is available in the online journal.)

the asymmetries in $H\alpha$ line could be produced by the strong velocity gradients in the chromosphere generated by the evaporation and condensation processes (e.g., Abbett & Hawley 1999, Kuridze et al. 2015). The velocity gradients create differences in the opacity between the red and blue wings of $H\alpha$, and the sign of the gradient determines whether the asymmetric emission appears to the blue or red side of the line profile. One explanation of the blue asymmetry is that if the downflow occurs in the upper chromosphere, its effect would be a red wing absorption, which can lead to a blue asymmetry in the line profile (e.g., Canfield et al. 1990, Gan et al. 1993, Heinzel et al. 1994, Kuridze et al. 2015). Another explanation is that a cool dense plasma moves upward via chromospheric evaporation and filament activation during the early or late phase of the flare (e.g., Canfield et al. 1990, Allred et al. 2006, Huang et al. 2014, Tei et al. 2018). These three models can explain solar flares whose blue asymmetry is seen only in the early or late phase. However, the blue asymmetry in this observation is different from the solar one. It was present during the whole period, from the early phase to the later phase of the flare. The blue asymmetry in the decay phase can be explained by the absorption by downward-moving plasma of post-flare loops in the corona, although this model cannot explain the blue asymmetry in the early phase. As we described above, there are many studies illustrating how blue asymmetry is generated during solar flares. However, there is no definite proof of any of them, and possibly newly developed ideas are necessary for a more detailed understanding. This observation can not determine the origin of the blue asymmetry, but it will give important clues for understanding flare dynamics and radiation mechanisms.

A sharp absorption component is seen in the red part of the $H\alpha$ line in the early and later phases of the flare during the observation. The velocity of this absorption did not change during the flare, but the strength seemed to change. This absorption component might be caused by plasma downflows produced (condensation patterns) in the post-flare loops. In this case, the plasma flow produced by previous flares gets cold and descends. Schmieder et al. (1987) shows the observed $H\alpha$ line profiles in post-flare loops on the Sun, and similar absorption features can be seen with similar velocity components as we observed. Canfield et al. (1990) also shows the blue- and red-shifted absorption features in an eruption of a filament on the Sun in the early phase of a flare. Cao & Gu (2012) found several absorption features of the $H\alpha$ region in the subtracted spectra of a very active RS CVn-type star. The absorption features can be explained by cool post-flare loops projected against the bright flare background, which sometimes occur during the gradual decay phase of large two-ribbon solar flares and can last for up to several hours (Wiik et al. 1996; Jing et al. 2016).

We discussed the observed stellar flare considering several solar flare studies. On the observations of solar flares, it is performed in various wavelength regions with high spatial resolutions, and detailed information are obtained. In order to apply the solar flare models to the stellar flare, more de-

tailed observations are required. The detailed observation with time and spatial cadence comparable to the solar case is difficult for the observations of stellar flares, but high-dispersion spectroscopy and multi-band observations will be useful for the studies of flare mechanism in detail.

5 Summary

We observed the dMe flare star EV Lac with a medium-resolution spectrograph mounted on the Nayuta telescope. The equivalent width of the $H\alpha$ emission showed substantial changes during our observation period. On August 15, 2015, we observed a rapid rise and the following slow decrease of the emission-line intensity of $H\alpha$, which was probably caused by a flare. The profiles of $H\alpha$ during the flare exhibited blue asymmetry and an absorption component in the red wing of the emission line. In contrast to the solar flares where blue asymmetries are mainly reported during the early phase of the flare, we observed it during the whole duration of the flare. We note that the blue asymmetry has also been produced during the late stage of solar flare events due to the filament activation/eruption and evaporation. We speculate that the blue asymmetries in EV Lac presented in this work is likely to be the analog to solar observations that report the blue asymmetries in the flare profiles. The absorption component seen in the red part of the emission may be caused by plasma downflows produced (condensation patterns) in the post-flare loops. However, there is no definite proof of either interpretation at the present. In order to understand the gas dynamics during flares, spectroscopic observations with higher spectral and temporal resolution are necessary.

Acknowledgments

We would like to thank Dr. Petr Heinzel for the discussions on the interpretation of the results, Drs. Suzanne L. Hawley, and Adam F. Kowalski also, for their helpful comments on the work. We also thank the staff of NHAO. We also thank an anonymous referee for many helpful comments. This work was supported by the Grant-in-Aids from the Ministry of Education, Culture, Sports, Science and Technology of Japan (No. 26400231, 16H03955, 16J00320, 16J06887, 17K05400, and 17H02865).

References

- Abbett, W. P., & Hawley, S. L. 1999, *ApJ*, 521, 906
- Alekseev, I. Yu., Baranovskii, E. A., Gershberg, R. E., et al. 2003, *Astron. Rep.*, 47, 312
- Allred, J. C., Hawley, S. L., Abbett, W. P., & Carlsson, M. 2006, *ApJ*, 644, 484
- Baranovskii, E. A., Gershberg, R. E., & Shakhovskoi, D. N. 2001a, *Astron. Rep.*, 45, 309
- Caballero-Garcia, M. D., Simon, V., Jelinek, M., et al. 2015, *MNRAS*, 452, 4195

Candelaresi, S., Hillier, A., Maehara, H., Brandenburg, A., & Shibata, K. 2014, ApJ, 792, 67

Canfield, R. C., Cheng, C., Dere, K. P., et al. 1980, in Skylab Solar Workshop II, ed. P. A. Sturrock, 451-469

Canfield, R. C., Kiplinger, A. L., Penn, M. J., & Wulser, J.-P. 1990, ApJ, 363, 318

Cao D.-T., Gu S.-H., 2012, A&A, 538, A130

Crespo-Chacon, I., Montes, D., Garcia-Alvarez, D., et al. 2006, A&A, 452, 587

Davenport, J. R. A. 2016, ApJ, 829, 23

Eason, E. L. E., Giampapa, M. S., Radick, R. R., Worden, S. P., & Hege, E. K. 1992, AJ, 104, 1161

Favata, F., Reale, F., Micela, G., Sciortino, S., Maggio, A., & Matsumoto, H. 2000a, A&A, 353, 987

Gan, W. Q., Rieger, E., & Fang, C. 1993, ApJ, 416, 886

Gunn, A. G.; Doyle, J. G.; Mathioudakis, M.; Avgoloupis, S. 1994, A&A, 285, 157

Gunn, A. G.; Doyle, J. G.; Mathioudakis, M.; Houdebine, E. R.; Avgoloupis, S. 1994, A&A, 285, 489

Ichimoto, K. & Kurokawa, H. 1984, SoPh, 1984, 93, 105

Haisch B., Strong K. T., Rodono A M., 1991, ARA&A, 29 275

Hawley, S. L. & Pettersen, B. R. 1991, ApJ, 378, 725

Hawley, S. L., Walkowicz, L. M., Allred, J. C., & Valenti, J. A. 2007, PASP, 119, 67

Hawley, S. L., Davenport, J. R. A., Kowalski, A. F., et al. 2014, ApJ, 797, 121

Heinzl, P., Karlicky, M., Kotrc, P., & Svestka, Z. 1994, SoPh, 152, 393

Hoidebine, E. R., Foing, B. H., Doyle, J. G., Rodono, M. 1993, A&A, 274, 245

Hoidebine, E. R., et al. 2009, A&A, 503, 929

Huang, Z., et al. 2014, A&A, 566, 148

Jing, J., Xu, Y., Cao, W., et al. 2016, Scientific Reports, 6, 24319

Johns-Krull, C. M., Hawley, S. L., Basri, G., & Valenti, J. A. 1997, ApJS, 112, 221

Kowalski, A. F., Hawley, S. L., Holtzman, J. A., Wisniewski, J. P., & Hilton, E. J. 2010, ApJ, 714, L98

Kuridze, D. et al. 2017, ApJ, 846, 9

Kuridze, D. et al. 2016, ApJ, 832, 147

Kuridze, D. et al. 2015, ApJ, 813, 125

Maehara, H., et al. 2012, Nature, 485, 478

Martin, E. L. 1999, MNRAS, 302, 59

Melikian, N. D., Tamazian, V. S., Docobo, J. A., Karapetian, A. A., Natsvlshvili, R. Sh. 2006 Astrophysics, 49, 488

Maehara, H., et al. 2015, EP&S, 67, 59

Namekata, K., et al. 2017, ApJ, 851, 91

Notsu, Y., et al. 2013b, ApJ, 771, 127

Osten R. A. et al 2010 ApJ 721 785

Pettersen, B. R. 1980b, AJ, 85, 871

Schaefer, B. E., King, J. R., & Deliyannis, C. P. 2000, ApJ, 529, 1026

Schmidt, S. J., Kowalski, A. F., Hawley, S. L., et al. 2012, ApJ, 745, 14

Schmieder, B., Forbes, T. G., Malherbe, J. M., & Machado, M. E. 1987, ApJ, 317, 956

Shibata, K., & Yokoyama, T. 2002, ApJ, 577, 422

Shibata, K., & Magara, T. 2011, Living Rev. Sol. Phys, 8, 6

Shibata, K., et al. 2013, PASJ, 65, 49

Shibayama, T., et al. 2013, ApJS, 209, 5

Tei, A., et al. 2018, PASJ, in press (arXiv.1803.05237)

Weaver, W. B., & Naftilan, S. A. 1973, PASP, 85, 213

Wiik, J. E., Schmieder, B., Heinzel, P., & Roudier, T. 1996, SoPh, 166, 89

Yang, H. 2017 ApJ 849 36

Table 1. Observing Log

Obs. date	Start-End time(JST)	Observation Duration (hours)	Exp. Time (sec)	Number of spectra
2015-07-31	25h 46m - 25h 56m	0.17h	600s	1
2015-08-01	27h 22m - 28h 15m	1h	300s	10
2015-08-15	25h 41m - 28h 26m	2.5h	300s	30
2015-08-26	22h 25m - 27h 56m	5.5h	180s	100
2015-08-27	24h 48m - 28h 10m	3.5h	180s	60

Table 2. The measured equivalent widths and observation date. (This table is available in its entirety in machine-readable form.)

Obs. date(JD)	E.W.(Å)	Obs. date(JD)	E.W.(Å)
July 31			
2457235.19861	3.22		
August 1			
2457236.13819	2.91	2457236.14167	3.12
2457236.14514	3.03	2457236.14931	2.90
2457236.15278	3.09	2457236.15764	3.02
2457236.16111	2.90	2457236.16528	2.76
2457236.16875	2.99	2457236.17292	2.96
August 15			
2457250.19514	7.96	2457250.19861	7.90
2457250.20208	8.10	2457250.20625	8.26
2457250.20972	8.25	2457250.21319	8.42
2457250.21667	9.04	2457250.22014	10.17
2457250.22431	10.36	2457250.22802	10.47
2457250.23164	10.43	2457250.23527	9.76
2457250.23888	9.87	2457250.24250	9.47
2457250.24625	9.66	2457250.25491	9.56
2457250.25852	9.66	2457250.26214	9.29
2457250.26575	9.25	2457250.26938	9.14
2457250.27300	8.70	2457250.27662	8.97
2457250.28024	9.10	2457250.28385	8.78
2457250.28748	8.31	2457250.29113	8.78
2457250.29476	8.41	2457250.29837	8.82
2457250.30204	8.63	2457250.30565	9.06
August 26			
2457261.05948	3.95	2457261.06171	3.86
2457261.06395	4.03	2457261.06618	3.82
2457261.06841	3.98	2457261.07064	4.04
2457261.07287	4.00	2457261.07509	4.05
2457261.07733	3.90	2457261.07955	4.01
2457261.08186	4.00	2457261.08409	4.31
2457261.08632	4.17	2457261.08855	4.29
2457261.09078	4.26	2457261.09331	4.35
2457261.09559	4.67	2457261.09791	4.94
2457261.10013	4.68	2457261.10236	4.83
2457261.10466	4.80	2457261.10689	4.85
2457261.10912	4.89	2457261.11134	4.66